Autologous Umbilical Cord Blood–Derived Mononuclear Cell Therapy Promotes Cardiac Proliferation and Adaptation in a Porcine Model of Right Ventricle Pressure Overload

Saji Oommen[1]* , **Susana Cantero Peral[1]***, **Muhammad Y. Qureshi[2]*** , **Kimberly A. Holst[3]**, **Harold M. Burkhart[4]**, **Matthew A. Hathcock[5]**, **Walter K. Kremers[5]**, **Emma B. Brandt[1]** , **Brandon T. Larsen[6]**, **Joseph A. Dearani[3]**, **Brooks S. Edwards[7]**, **Joseph J. Maleszewski[8]**, **Timothy J. Nelson[1]**, and **Wanek Program Pre-Clinical Pipeline[†]**

Abstract

Congenital heart diseases, including single ventricle circulations, are clinically challenging due to chronic pressure overload and the inability of the myocardium to compensate for lifelong physiological demands. To determine the clinical relevance of autologous umbilical cord blood–derived mononuclear cells (UCB-MNCs) as a therapy to augment cardiac adaptation following surgical management of congenital heart disease, a validated model system of right ventricular pressure overload due to pulmonary artery banding (PAB) in juvenile pigs has been employed. PAB in a juvenile porcine model and intramyocardial delivery of UCB-MNCs was evaluated in three distinct 12-week studies utilizing serial cardiac imaging and end-of-study pathology evaluations. PAB reproducibly induced pressure overload leading to chronic right ventricular remodeling including significant myocardial fibrosis and elevation of heart failure biomarkers. High-dose UCB-MNCs (3 million/kg) delivered into the right ventricular myocardium did not cause any detectable safety issues in the context of arrhythmias or abnormal cardiac physiology. In addition, this high-dose treatment compared with placebo controls demonstrated that UCB-MNCs promoted a significant increase in Ki-67-positive cardiomyocytes coupled with an increase in the number of CD31+ endothelium. Furthermore, the incorporation of BrdU-labeled cells within the myocardium confirmed the biological potency of the high-dose UCB-MNC treatment. Finally, the cell-based treatment augmented the physiological adaptation compared with controls with a trend toward increased right ventricular mass within the 12 weeks of the follow-up period. Despite these adaptations, functional changes as measured by echocardiography and magnetic resonance imaging did not demonstrate differences between cohorts in this surgical model system. Therefore, this randomized, double-blinded, placebo-controlled pre-clinical trial establishes the safety of UCB-MNCs delivered via intramyocardial injections in a dysfunctional right ventricle and validates the induction of cardiac proliferation and angiogenesis as transient paracrine mechanisms that may be important to optimize long-term outcomes for surgically repaired congenital heart diseases.

Keywords

congenital heart disease, pulmonary artery banding, umbilical cord blood–derived mononuclear cells, cardiac adaptation, proliferation

[1] Division of Cardiovascular Diseases, Center for Regenerative Medicine, Mayo Clinic, Rochester, MN, USA
[2] Division of Pediatric Cardiology, Mayo Clinic, Rochester, MN, USA
[3] Department of Cardiovascular Surgery, Mayo Clinic, Rochester, MN, USA
[4] Pediatric Cardiothoracic Surgery, The University of Oklahoma, Oklahoma City, OK, USA
[5] Biomedical Statistics and Informatics, Mayo Clinic, Rochester, MN, USA
[6] Laboratory Medicine and Pathology, Mayo Clinic, Scottsdale, AZ, USA
[7] Transplant Center, Mayo Clinic, Rochester, MN, USA
[8] Anatomic Pathology, Mayo Clinic, Rochester, MN, USA

* Oommen, Cantero Peral, and Qureshi contributed equally to this work.

Corresponding Author:
Timothy J. Nelson, Division of Cardiovascular Diseases, Center for Regenerative Medicine, Mayo Clinic, 200 First Street, SW, Rochester, MN 55905, USA.
Email: nelson.timothy@mayo.edu

Introduction

Congenital heart disease (CHD) affects ~0.1% of live births in the United States annually[1]. Clinical challenges facing patients and providers have evolved as survival during infancy, and early childhood has improved[2]. Over three decades, single ventricle palliative surgery has provided life-saving opportunities for severe CHD patients[3,4]. At the same time, palliative surgeries also create unmet needs for this young patient population that have survived these surgeries. It has been contemplated that the single morphologic right ventricle (RV) has a lower adaptation to ventricular volume overload during required surgeries[5]. An abnormal RV contractility and function have been seen after insufficient compensatory hypertrophy of ventricles (mass/volume ratio)[6]. Late sequela of suboptimal cardiac performance contributes to detrimental effects on the organs like lungs, kidneys, and liver. Furthermore, cardiac transplantation is limited by a 20% and 30% mortality rate at 1 and 5 years, respectively, for patients with failing single ventricle hearts[7]. The development of a therapeutic strategy to improve single ventricular function and delay the need for cardiac transplantation will require robust pre-clinical animal models to establish the evidence of safety and efficacy relevant to pediatric applications.

Currently, there is no pre-clinical model system that mimics the hemodynamic stress caused by sustained pressure overload to the RV, thus recapitulating the stress on the myocardium of an infant with single-ventricle CHD. Ideally, the pre-clinical model would reflect the growth and development of a juvenile heart with myocardial remodeling occurring over a long period of time to mimic the true pathophysiology in a pediatric setting. Herein, we have developed a reproducible porcine model system using pulmonary artery banding (PAB), within the first few weeks of life to optimize a therapeutic trial design within a neonatal circulatory system relevant to the current surgical management of CHD. We have established a strong track record of safety and demonstrated the augmentation of adaptive cellular responses that could be applicable to transform the care of a broad spectrum of CHD patients requiring palliative reconstructive surgery[8,9]. Umbilical cord blood (UCB) stem cells are a particular source of multipotent stem cells for regenerative purposes and have been tested in numerous cardiovascular conditions[10–12]. UCB-derived cells have been examined in the context of damaged tissues given their association with proliferative potential, multi-lineage differentiation, pro-angiogenic function, and anti-inflammatory/regenerative capacity[13–16]. Herein, we applied a double-blinded, randomized placebo-controlled study to determine the safety and effectiveness of UCB-derived cells using an intramyocardial surgical delivery in the setting of right pressure overload in a porcine model.

Materials and Methods

Animal Selection

Pregnant female swine of Large White/Landrace breed background were obtained from an independent vendor. According to the approved Institutional Animal Care and Use Committee (IACUC) protocol, piglets were born and weaned at a Mayo Clinic animal house facility. Piglets of either sex (4–8 kg body weight) were assigned to respective groups that were chosen, first, to establish the reproducibility of the model system and, second, to conduct a randomized controlled trial (RCT). All the animals used in this study received care in compliance with the National Research Council Guide for the *Care and Use of Laboratory Animals*.

UCB Collection, Isolation, and Cryopreservation of UCB-MNCs

Pregnant sows and gilts underwent induced labor or non-survival C-sections, respectively, at approximately day 115 of gestation. Surgical delivery of piglets allowed UCB collection for individual piglets. The UCB was processed within 24 h using the Ficoll density gradient as described previously with identical release criteria[9]. Product characterization included sterility culture (aerobic and anaerobic) and flow cytometry analysis [total nucleated cell (TNC) count, mononuclear cell (MNC) percentage by forward scatter (FSC)/side scatter (SSC), and 7-aminoactinomycin D (7-AAD) viability]. The final cell-based product (UCB-MNCs) was stored in a sterile cryopreservation medium containing 10% dimethyl sulfoxide (DMSO) at a concentration of 30×10^6 TNC/ml.

Quality Control Assays

Quality control assays were carried out in cord blood samples not used in animals that were randomized to the placebo group or that had extra vials to assure that the resulting data were of sufficient quality and integrity. The viability of the cells immediately after being thawed was analyzed by flow cytometry. Briefly, samples were thawed at 37°C for 4 to 5 min, and 7-AAD vital dye was added to the cells and incubated for 15 min at room temperature. The samples were run in a FACSCan flow cytometer (Beckton, Dickinson and Company, Franklin Lakes, NJ, USA), and the data analysis was immediately performed using the CellQuest Software (BD Biosciences FACS series instruments, San Jose, CA, USA).

Overview of Study Design

Weaned piglets at 3 to 4 weeks of age from seven litters were sequentially examined in a series of studies: *Study 1* established the natural history of PAB and right ventricular dysfunction (Fig. 1A); *Study 2* evaluated the cardiac safety and feasibility of several doses of autologous UCB-MNCs (Fig. 3A), and *Study 3* assessed the efficacy of the highest safe dose of autologous UCB-MNCs transplantation in a diseased RV (Fig. 5A). All piglets were randomly allocated to seven groups (pairwise comparison of A vs B for each of the three studies) as Group 1A sham operation ($n = 8$), Group 1B PAB ($n = 13$), Group 2A PAB + UCB-MNCs (0.3 million cells/kg)

($n = 5$), Group 2B PAB + UCB-MNCs (1 million cells/kg) ($n = 6$), Group 2C PAB + UCB-MNCs (3 million cells/kg) ($n = 4$), Group 3A PAB + placebo DMSO administration ($n = 9$), and Group 3B PAB + UCB-MNCs ($n = 7$).

Groups 1A/B: Development and validation of a porcine model of PAB to induce RV pressure overload: PAB is a palliative clinical surgical correction procedure for the treatment of patients with CHD. Randomized piglets (Group 1A and 1B) underwent either a sham control operation with left thoracotomy to expose the pericardium (no PAB) or surgical PAB, respectively. PAB was performed at ~4 weeks of age when the piglets were ~6 kg body weight and followed for 12 weeks.

Group 2 A/B/C: Safety and feasibility of UCB-MNCs dose-escalation transplantation in diseased RV: This study presents the safety of intramyocardial delivery of MNCs and feasibility in a porcine model with chronic pressure overload. Randomized double-blinded piglets (Groups 2A, 2B, and 2C) all underwent surgical PAB at ~4 weeks of age followed by intramyocardial injections through a second right-sided thoracotomy 2 weeks after the PAB procedure. Group 2A was treated with autologous UCB-MNCs at 0.3 million, group 2B at 1 million, and group 2C at 3 million/kg, respectively, with direct intramyocardial injections into the lateral free wall at the basal level of the right ventricle. Animals were studied for 12 weeks post-cell transplantation.

Group 3 A/B: Efficacy of autologous UCB-MNCs intramyocardial transplantation. Animals were randomly assigned in a double-blinded fashion once right ventricular stress was documented on echocardiography by a mean Doppler gradient of at least 25 mm Hg across the PAB. Intramyocardial injections were performed 2 weeks after PAB at ~6 weeks of age. Group 3A received a dose of DMSO (placebo) and Group 3B received MNCs (3×10^6 TNC/kg) with direct intramyocardial injections into the lateral free wall of the right ventricle. Animals were sacrificed at 12 weeks post intramyocardial injections for histological assessments.

Surgical Procedures: PAB

General anesthesia was induced in piglets by intramuscular injection of tiletamine HCl and zolazepam HCl (5 mg/kg) with xylazine (1–2 mg/kg) and maintained on isoflurane via endotracheal intubation. Following the administration of anesthesia, a left anterolateral chest surgery was performed through the fourth or fifth intercostal space. Banding of the pulmonary trunk was performed with umbilical cord tape, approximately 1 cm distal to the sinotubular junction. The degree of the pulmonary obstruction was progressively adjusted by monitoring direct intraventricular pressure with a transducer to evaluate the systolic RV pressure. An elevation of the systolic RV maximal pressure of 40% to 60% above the basal level was typically

achieved with PAB. A fluid bolus of 20 ml/kg body weight before tightening the band was added before PAB for Group 3 to advance the reproducibility of the pressure overload phenotype. The chest cavity was closed in layers, and animals were returned to the postoperative room for care and recovery.

Autologous UCB-MNCs Transplantation into the Right Ventricle Myocardium

The piglets in Groups 2 and 3 were randomized to placebo or UCB-MNCs treatment. A right-sided thoracotomy in the fifth to sixth intercostal space was used to expose the right ventricle lateral free wall near the basal level for single-dose injection. The number of injections (0.1 ml/injection) matched the kilogram of every animal. In Group 2, the cryopreserved autologous UCB-MNCs at a concentration of 30 million cells/ml were thawed and the dose was adjusted depending on the cell concentration group-randomized. In group 2C (3 million cells/kg), cells were delivered into the myocardium within 20 min without further manipulation. In Groups 2A and 2B, cells were diluted 3- or 10-fold for a final concentration of 1 million cells/kg and 0.3 million cells/kg, respectively. Cells were diluted with DMSO in a clean safety hood next to the operation room. In Group 3, the cryopreserved autologous UCB-MNCs at a 30 million/ml concentration were thawed and delivered without further manipulation into the myocardium within 20 min. The UCB-MNCs were administered in 0.1 ml aliquots at several injections to achieve a dose of 3×10^6 cells/kg (maximal dose used in clinical studies). The injection sites were arranged in a radial pattern aiming outwards; the inner diameter of the puncture site pattern was ~2 cm.

Echocardiography

Two-dimensional echocardiography was used to evaluate cardiac function in all animals (GE Vivid 7 ultrasound system, Milwaukee, WI, USA). A simultaneous electrocardiogram was recorded using three-limb leads. Triplicate measurements were made off-line using EchoPAC (version 112.01, GE Healthcare, Milwaukee, WI, USA). Multiple parameters for quantification of RV function were recorded which included apical fractional area change (FAC), myocardial performance index (MPI), tricuspid valve lateral annular tissue velocities, tricuspid annular plane systolic excursion (TAPSE), and isovolumic acceleration (IVA). The mean Doppler gradient across the PAB was measured. The right ventricular systolic pressure by tricuspid valve regurgitation velocity was estimated in a standard clinical fashion.

Magnetic Resonance Imaging

Piglets were sedated and intubated to maintain breath holds during image acquisition using 1% to 2% inhaled isoflurane and withholding ventilations. All cardiac magnetic resonance

imaging (MRI) was performed on a 1.5 Tesla scanner (General Electric Signa). All animals were imaged supine. Electrocardiographic leads were placed on the anterior chest. Stacks of cine images (steady-state free precession) in short-axis planes were acquired for ventricular volume assessments and ejection fraction (EF). Imaging parameters were optimized based on the animal size to maintain an in-plane resolution of 1.5 to 2 mm. These included a field of view of 26 to 36 cm, phase field of view of 0.6 to 1, frequency 130 to 240 mm, and phase 78 to 240 mm. Phase-contrast images were recorded for flow quantification at the proximal ascending aorta and proximal main pulmonary artery. Encoding velocity was set at 2 m/s by default and was increased if aliasing occurred. Gadolinium-enhanced angiography was performed to assess the pulmonary arteries. Post-contrast images were obtained 6 min after contrast injection to assess delayed myocardial enhancement. Flow quantification and calculation of ventricular volumes and ejection fractions were performed on cvi[42] (release 5.3.4, Circle Cardiovascular Imaging, Calgary, Alberta, Canada). End-diastolic and systolic volumes of both ventricles were calculated by planimetry on the short-axis cine stack. Next, pulmonary and systemic blood flows were measured by flow quantification across the pulmonary artery and ascending aorta, respectively. Antegrade flow across the pulmonary artery was accounted for the effective stroke volume of the RV and was used to calculate the effective ejection fraction (eEF) (effective stroke volume/end-diastolic volume $\times$ 100). Three-dimensional reconstruction of images and double oblique measurements were obtained on Aquarius iNtuition software (v. 4.4.8, TeraRecon, San Mateo, CA, USA).

In Vivo *Bromodeoxyuridine Assay to Characterize Cell Proliferation*

To monitor cardiomyocyte proliferation, bromodeoxyuridine (BrdU), a thymidine analog cell proliferation marker, was administered. Every animal included in Group 2 received 50 mg/kg intravenous BrdU dissolved in lactated Ringer solution 24 h before sacrifice. Cardiac tissue was collected during necropsy, 12 weeks post cell injection, for immunohistochemical analysis. To count the BrdU-positive proliferating cardiomyocytes, images were taken at 40$\times$ magnification, counted manually, and reported as absolute counts of cells/mm^2.

Natriuretic Peptides (BNP and ANP) Detection and Cardiac Histology

Cardiac-specific biomarkers of heart failure were evaluated in plasma at multiple time points. According to the pre-determined study protocol, these markers included N-terminal brain natriuretic peptide (BNP) and atrial natriuretic peptide (ANP) and were assessed via an immune-radiometric assay. The heart was dissected and tissue from the free wall of the

RV and LV, and the interventricular septum, was obtained, and 10% neutral-buffered formalin was used as a fixative. The deparaffinized tissue sections were stained with hematoxylin and eosin (H&E) and Masson's trichrome to assess for the presence of any lesions and/or fibrosis. Stained sections were imaged at 40$\times$ magnification by bright-field light microscopy. Intestinal samples were also collected for each animal in the Group 2 to ensure BrdU incorporation.

Immunohistochemistry and Immunofluorescence

The right ventricular tissue from normal, placebo, and cell-treated groups were used for immunohistochemistry (IHC) staining using antibodies directed against the proliferation markers BrdU and Ki-67. For Ki-67 staining (clone MIB-1, Dako), standard clinical laboratory protocols on an automated immunohistochemistry platform (Bond RX, Leica Biosystems, Buffalo Grove, IL, USA) were used. The BrdU slides were double stained with cardiac marker troponin T to differentiate BrdU incorporation into cardiomyocytes versus non-cardiomyocytes cells. A monoclonal BrdU antibody from Abcam, clone BU1/75 [ICR1] (ab6326), and a monoclonal anti-cardiac troponin T antibody (red chromogen), clone 1F11 (ab10214) were used. A mouse monoclonal antibody against CD31/PECAM-1, an endothelial marker (Santa Cruz Biotechnology, Santa Cruz, CA, USA) was used to detect vascular endothelium. The slide images were scanned using the Aperio ScanScope (Leica Biosystems, Buffalo, Grove, IL, USA). Blinded Ki-67 analysis was performed using validated nuclear algorithm software (Aperio ImageScope, Leica Biosystems, Nussloch, Germany). The porcine heart sections were deparaffinized using standardized immuno-fluorescence (IF) protocols, and antigen retrieval was performed using citrate buffer. Sections were stained overnight with anti-cardiac troponin antibody (Mouse IgG Monoclonal, 1:1,000, Thermo Fisher Scientific, Waltham, MA, USA) and anti-Ki-67 antibody (Rabbit IgG Polyclonal 1:2,000, Abcam, Cambridge, MA, USA), then washed and stained with secondary Alexa Fluor 400 Donkey anti-Mouse [IgG (H + L), 1:2500, Life Technologies, Carlsbad, CA, USA]. The images were acquired using the Zeiss LSM780 microscope (40$\times$ Water Objective, NA 1.2).

Real-Time PCR Assay

PCR analysis was performed using RNA extracted from the mouse heart (free wall of the RV) using RNeasy Plus Mini Kit (Qiagen, Valencia, CA, USA). The reverse transcriptase (RT) was performed with an iScript cDNA reaction kit (Bio-Rad, Hercules, CA, USA). Quantitative assessment of predictive cardiac markers: *MYH7*, *GATA-4*, *KDR*, *Mef2c*, Acta1, SRF, alpha-MHC, Nkx2.5, and *WT1* (Bio-Rad) was performed. The gene expression values were normalized to the *GAPDH* values and are expressed as 2$-\Delta\Delta$Ct (fold change).

Statistical Analysis

Continuous variables obtained at different time points were described by mean $\pm$ SD or median and interquartile range as appropriate; categorical variables by counts and percentages. A box and whisker plot is used for graphical display, highlighting the median and interquartile. Comparisons between the treatment (PAB or MNCs) and control groups were performed by using a *t*-test for continuous variables and chi-square or Fisher exact tests for categorical variables. The pre-and post-treatment analyses were analyzed using a paired *t*-test. Using ascites as the clinical marker of right heart failure, subgroup analysis was performed to assess the association between the presence of ascites with imaging and biochemical markers, again based upon *t*-tests and chi-square or Fisher exact tests, as appropriate. Two-way analysis of covariance (ANCOVA) was performed on MRI, echocardiography, and demographic data for comparison between the treatment and control groups across all the time points (weeks) after adjusting for the prior time point's measurement. Analyses were also performed using a statistical software system [GraphPad Prism (version 5, San Diego, CA, USA) and SAS 9.4 (Cary, NC, USA)], and a *P*-value of less than 0.05 was considered statistically significant; no adjustments were made for multiple testing.

Results

Natural History of Right Ventricular Function Following Permanent Banding of the Pulmonary Artery in Juvenile Pigs

Groups 1A and 1B: Systolic RV pressures were immediately increased after PAB reduced the pulmonary artery to ~4 to 6 mm in diameter using umbilical cord tape and vascular surgical clips with the material finally secured into the outer wall of the pulmonary artery (PA) with a suture (Fig. 1A–C). After 12 weeks, MRI 3D reconstructions demonstrated the proximal location of the tight band on the main pulmonary artery (Fig. 1D, E) and the structural changes imposed on the RV compared with sham controls including right ventricular dilation and hypertrophy, as well as bowing of intraventricular septum toward the left ventricle (LV) signifying supra-systemic right ventricular systolic pressure (Fig. 1F–I).

Hemodynamic changes were documented between the sham and PAB cohorts by echocardiography demonstrating persistent PAB gradient and increased tricuspid regurgitation jet velocity consistent with increased right ventricular systolic pressure (Fig. 2A–D). Progressive RV dilation in the PAB group was observed with a significant change post-banding in mean end-diastolic area (PAB 21 $\pm$ 6 cm^2; control 9 $\pm$ 2 cm^2; *P* = 0.002) and mean end-systolic area (PAB 13 $\pm$ 4 cm^2; control 4 $\pm$ 1 cm^2; *P* = 0.002). The right ventricular fractional area change (FAC) was significantly reduced in the PAB alone group at 12 weeks (39% $\pm$ 7% vs
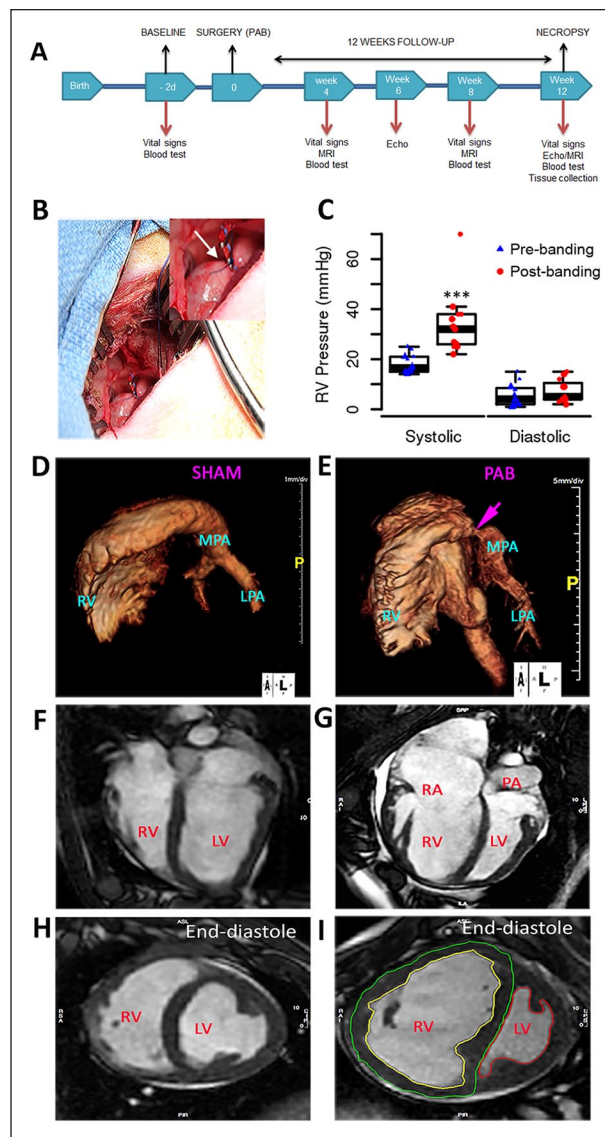

Figure 1. Study design and development of pressure overload PAB model: (A) Overview of experimental design. (B) Surgical exposure from left thoracotomy of the pulmonary artery with a band in position. (C) Acute RV systolic pressure elevated in response to PAB. (D–E) Images generated from a three-dimensional reconstruction of magnetic resonance angiogram of RV and pulmonary arteries from sham and PAB. (F–I) MRI characteristics of RV after 12 weeks of sham-operated and PAB. Four-chamber view of control (F) and a pulmonary artery banded animal (G) and short-axis plane at mid ventricle level (H, I) in end-diastole showing dilated RV with reduced systolic function and ventricular septum shift. Contouring of RV endocardium (yellow) and epicardium (green) as well as LV endocardium (red) is exemplarily shown (I). Echo: echocardiography; LPA: left pulmonary artery; LV: left ventricle; MPA: main pulmonary artery; MRI: magnetic resonance imaging; PA: pulmonary artery; PAB: pulmonary artery banding; RV: right ventricle; RA: right atrium.

50% $\pm$ 6% in the control group; *P* = 0.031). The mean right ventricular systolic pressure at 12 weeks was near/supra-systemic in the PAB group with a peak tricuspid valve
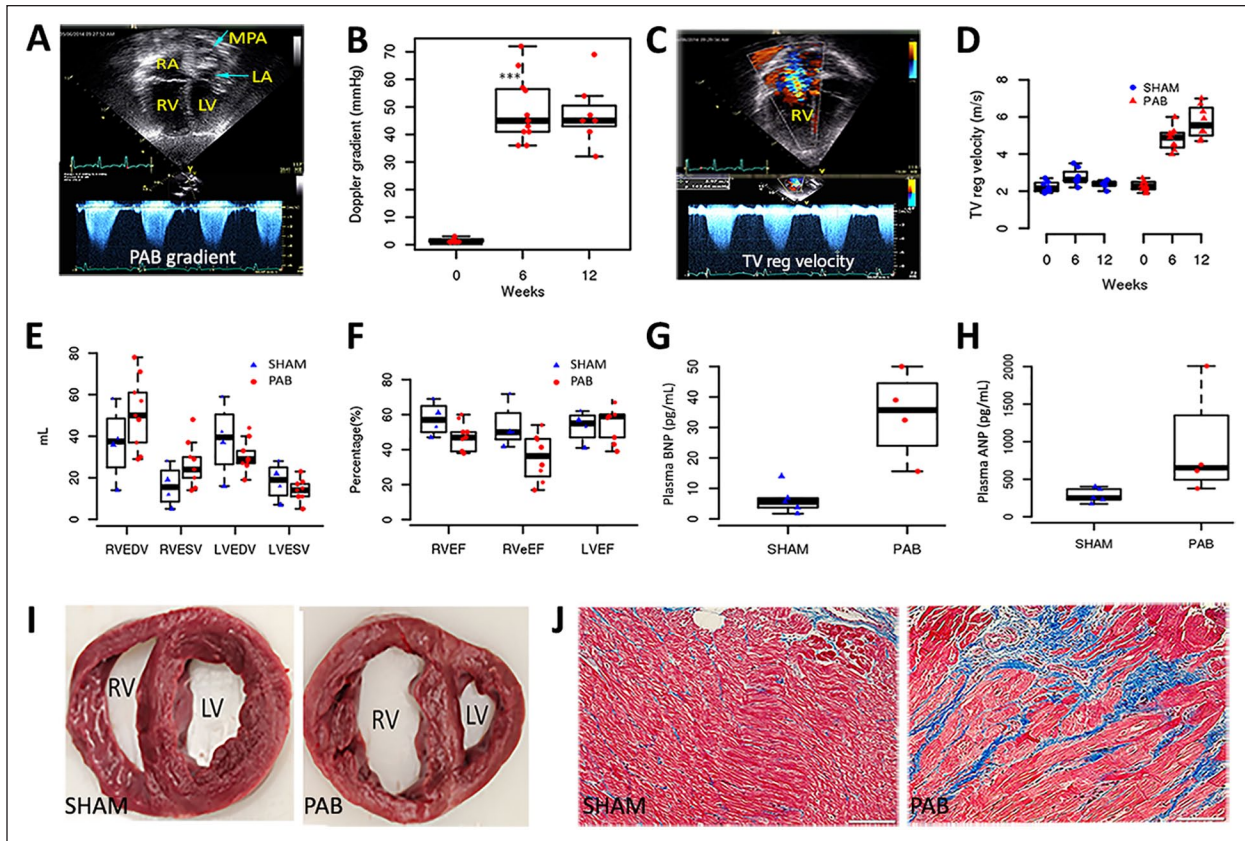
Figure 2. Validation of a juvenile porcine model of chronic right ventricular pressure overload: (A) Apical four-chamber view of an animal with PAB showing a dilated right atrium and RV. (B) Continuous-wave Doppler signals across the PAB showed a mean Doppler gradient of 48 mm Hg, which remained stable at weeks 6 and 12 post-PAB. (C) Apical four-chamber view with color Doppler showed severe tricuspid valve regurgitation, which (D) increased TV regurgitation velocity over 12 weeks post-PAB. (E) A comparison of volumetric analysis between the sham and PAB groups is shown in a bar graph. (F) A comparison of ventricular ejection fractions by volumetric analysis between the two groups is shown. (G) Circulating levels of BNP and (H) ANP were measured after 12 weeks of banding ($P < 0.001$, compared with the placebo group). (I) Gross morphological changes in sham and PAB heart. (J) Representative photomicrographs of Masson Trichrome staining of RV, showing interstitial fibrosis (blue). The scale bar represents 50 µM. ANP: atrial natriuretic peptide; BNP: B-type natriuretic peptide; LA: left atrium; LV: left ventricle; LVEDV: left ventricular end-diastolic volume; LVEF: left ventricular ejection fraction; LVESV: left ventricular end-systolic volume; MPA: main pulmonary artery; PAB pulmonary artery banding; RA: right atrium; RV: right ventricle; RVEDV: right ventricular end-diastolic volume; RVEF: right ventricular ejection fraction; RVeEF: right ventricular effective ejection fraction; RVESV: right ventricular end-systolic volume; TV reg: tricuspid valve regurgitation.

regurgitation jet velocity of 5.7 ± 0.9 m/s (control 2.4 ± 0.2 m/s, $P < 0.001$). The Doppler gradient average across the pulmonary artery band was 48 ± 12 mm Hg (peak gradient 80 ± 12 mm Hg). There was no significant difference in tricuspid valve inflow early diastolic velocity, RV myocardial performance index, RV isovolumic acceleration, and tricuspid valve annular early diastolic velocity between the two groups. The mean tricuspid annular systolic velocity measured by tissue Doppler imaging was significantly less in the PAB group (0.11 ± 0.02 m/s) compared with the control group (0.15 ± 0.02 m/s; $P = 0.004$). By MRI measurements, the indexed RV end-diastolic volume (RVEDV) and end-systolic volume (RVESV) increased progressively in the PAB group at each assessment interval (Fig. 2E). The mean right ventricle EF was significantly lower in the PAB group (48% ± 8%) than in the sham group (64% ± 9%;

$P = 0.003$) (Fig. 2F). The mean RV eEF was substantially lower in the PAB group (29% ± 15%) than in the placebo control group (60% ± 11%; $P < 0.001$) at the end of the study (Fig. 2F). The difference is more pronounced due to significant tricuspid valve regurgitation and a resultant decrease in effective stroke volume in the PAB group. Delayed myocardial enhancement at the septal ends of the RV free wall and/or interventricular septum was present in 63% of animals in the PAB group. No animal showed any discrete myocardial scars in the RV or LV walls. Furthermore, indicative of severe right heart failure, 38% of banded animals demonstrated ascites on MRI at the end of the study. None of the control animals showed any ascites or delayed myocardial enhancement.

Biomarkers of heart failure were significantly elevated after 12 weeks of PAB; BNP (sham 4.75 ± 1.25; PAB 34.3 ± 7.20;

$P = 0.01$) and ANP (sham 261 ± 37; PAB; 1,140 ± 321; $P= 0.03$; Fig. 2G, H). The clinical chemistry and hematology parameters were measured at different time intervals. No difference between PAB and sham was detected in clinical chemistry values. At the end of the study, animals were sacrificed, and heart tissue was collected for histological evaluation (Fig. 2I, J). Cardiomegaly was evident in the PAB group by the significantly higher wet weight of the heart (sham 185 ± 41 g; PAB 293 ± 77 g; $P = 0.01$). The right ventricular free wall muscle thickness was increased significantly in the PAB group ($P < 0.05$ at the base, mid, and apex). Masson's trichrome stain demonstrated interstitial fibrosis in the RV-free wall. The interventricular tricuspid valve annulus was progressively dilated in the PAB group and was significantly dilated at the end of the study (41 ± 7 mm vs 28 ± 5 mm in the control group; $P < 0.001$). The right atrium showed severe progressive dilation in the PAB group over the study duration with a substantially larger right atrial volume at the end of the study (17 ± 8 cm^3 vs 67 ± 27 cm^3 in the control group; $P = 0.001$).

Survival rate and adverse events: Four animals died due to anesthesia-related complications during follow-up imaging studies. Overall survival at the end of Study 1 was 88% (7/8) for the sham Group 1A and 62% (8/13) for the PAB Group 1B. Survival was improved during the subsequent imaging studies due to more vigilant monitoring of anesthesia during the MRI acquisition as the PAB cohort was hypersensitive given the degree of chronic right heart changes.

Myocardial Safety of Autologous UCB-MNCs Injection after Surgical Banding of Pulmonary Artery in Juvenile Pigs

Cord blood processing

Groups 2A, 2B, 2C. Umbilical cord blood was collected during C-section and processed according to standardized protocols and release criteria[9] (Fig. 3A). Autologous cell-based product characterization was confirmed before piglets were available for randomization (Fig. 3B, C). UCB was collected from 25 piglets before the placenta was delivered. UCB collected volume was 15 to 42 ml (mean = 30.4 ml, SD = 6.02 ml). One sample was discarded due to hemolysis. Twenty-four samples were then processed within 2 h of collection, and the TNCs that included the mononuclear cells were isolated and stored in liquid nitrogen until further use. TNC counts ranged from 11 × 10^6 cells to 62 × 10^6 cells (mean = 34.5 × 10^6 cells, SD = 15.49 × 10^6 cells). All animals met the minimum (50%) mononuclear cell percentage established in the release criteria (mean = 95.29%, SD = 5.33%). Viability >70% was also acquired in every animal (mean = 98.55%, SD = 0.9%). No microbiology contamination was encountered in any of the samples analyzed.

UCB-MNC quality control assays. After the cell/placebo injection into the pigs' right ventricle, 20 UCB samples that were not used in the animals because they were randomized to the placebo group or had extra vials were analyzed with mean post-thaw viability of 82%, SE = 1.1%. To account for that 18% of cell loss due to the process of freeze and thaw, all cord blood samples were frozen at a final concentration of 38 × 10^6 TNC/ml for a final viable target cell concentration of 30 × 10^6 TNC/ml (Fig. 3D).

Safety of intramyocardial injection of UCB-MNCs. Five animals were sacrificed before the first surgery due to low concentration of cells or health issues. Nineteen animals underwent PAB surgery. One animal died 3 days before the second surgery (cell injection surgery) due to heart failure. Fifteen out of 19 animals completed the study 12 weeks post-cell injection.

Cardiovascular tolerance studies using three UCB-MNCs doses (0.3 million/kg, 1 million/kg, and 3 million/kg) delivered into the myocardium of juvenile pigs after banding of pulmonary artery demonstrated their safety. Survival from the PAB surgery and intramyocardial injections was 79%, with lower mortality rates attributed to acute changes in hemodynamics and hypotensive shock. After 12 weeks of follow-up, all piglets in both groups tolerated research procedures without significant adverse events. Vital signs such as body temperature, respiratory rate, and body weights were not significantly different between the groups (Fig. 3E–G). The body temperature was analyzed as a health marker. It has shown a decrease in body temperature at the time of cell injection, independently of the dose, that returned to normal ranges within 48 h post-surgery (Fig. 3E). Cardiac troponin (TnI), plasma BNP, and ANP levels were measured after 12 weeks of treatment compared with baseline (Fig. 3H–J). We observed no significant changes in the level of any biomarker in all three dose levels compared with baseline (PAB-only pre-cell delivery) concentrations. However, we observed that some post-cell delivery ANP and BNP values were higher in the 1 million cells/kg and 3 million cells/kg groups. Since the PAB in this study intends to create a right heart pressure overload phenotype in the pigs when tightening a band around the pulmonary artery, we reviewed the necropsy results in those cases looking for signs such as ascites, pleural effusion, and macroscopic liver congestion. We also analyzed the pulmonary artery internal diameter at the band's site correlating all those parameters with the levels of ANP and BNP. Three out of six animals in the 1 million cells/kg group and 1 out of four in the 3 million cells/kg group had at least two times higher ANP and BNP levels post-cell delivery. They all showed signs of ascites, pleural effusion, and/or macroscopic liver congestion, not seen in the rest of the animals. Notably, the two animals with ANP levels higher than 700 pg/ml had a large volume of ascites (3900 and 4250 ml) and macroscopic liver congestion. The internal diameter of the pulmonary artery at the band site was reduced in the cases with higher ANP and BNP, compared to the rest of the animals (mean: 4.68 vs 5.61, SD: 0.6 vs 0.98, respectively, $P = 0.06$).
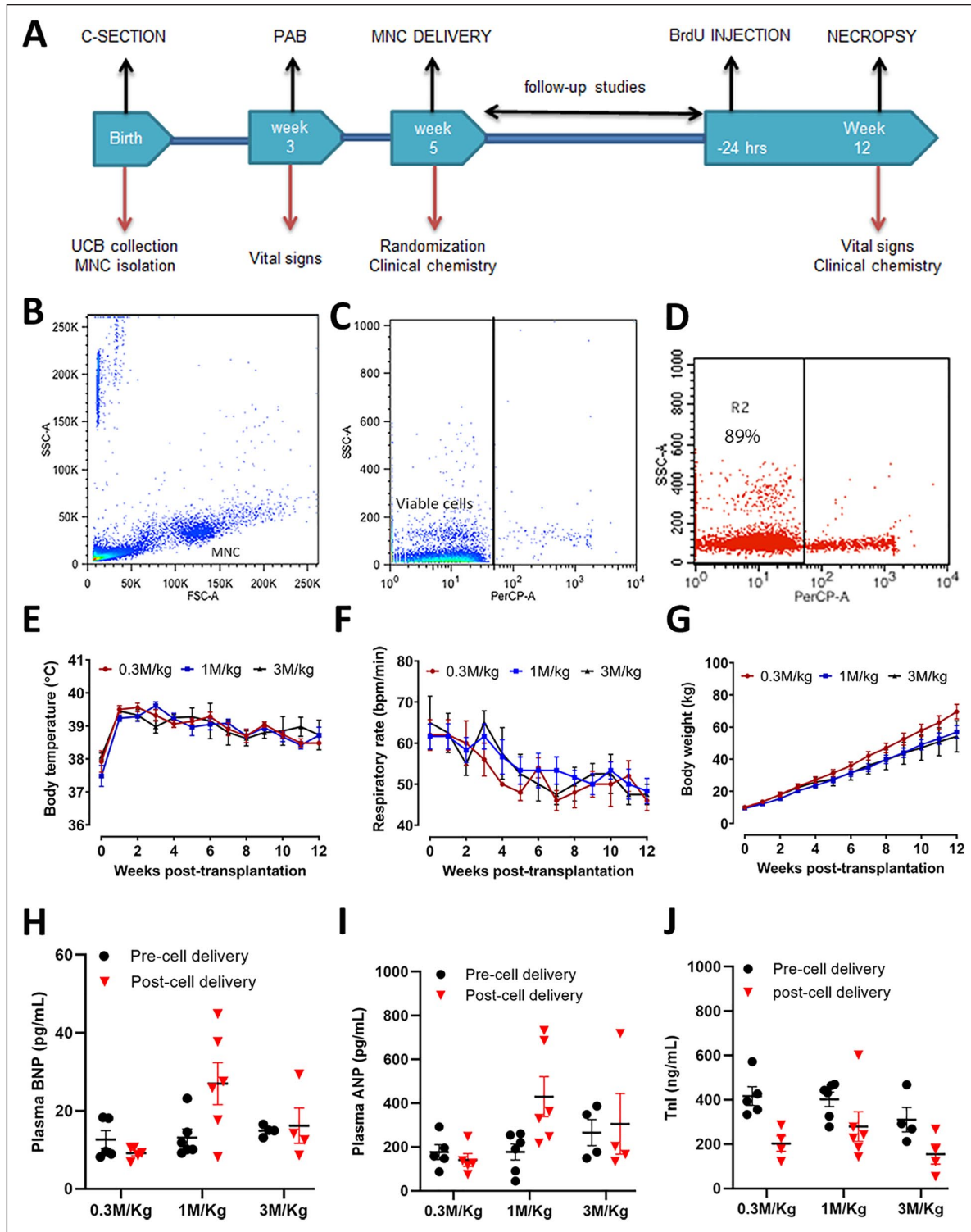
Figure 3. Study design and cardiac safety assessment of autologous porcine UCB-MNCs dose-escalation studies following intramyocardial delivery in acute right ventricular pressure overload. (A) Overview of experimental design. (B–D) The flowchart panel indicates the purity of mononuclear cells by flow cytometry. (E–G) Body temperature, respiratory rate, and body weight were recorded weekly from cell delivery (week 0–12). (H–J) Circulating levels of plasma BNP, ANP, and TnI were measured before cell delivery (2 weeks post-PAB) and at the end of the study (12 weeks post-cell delivery). ANP: atrial natriuretic peptide; BNP: B-type natriuretic peptide; BrdU: bromodeoxyuridine; C-section: cesarean section; FSC-A: forward scatter; M/Kg: millions per kilogram; MNC, mononuclear cells; PAB, pulmonary artery banding; SSC-A, side scatter; TnI, troponin I; UCB: umbilical cord blood.

No complications such as bleeding or infections were observed during the entire study. Blood samples collected during the study period did not detect any alterations in the hematological and biochemical analysis or differences within the three cell dose groups (Fig. S1).

Survival rate and adverse events. The autologous UCB-MNCs administration to the right ventricular muscle after PAB was feasible. The injections were challenging given the thin RV during the acute PAB stages, which did not represent chronic single ventricular morphology. Therefore, the subsequent study was designed to allow the RV to hypertrophy for 2 weeks before myocardial cell injections, which are more consistent with the clinical context of single ventricle heart surgeries. Furthermore, variability in PA gradients was thought to be due to a wide range of tolerated banding diameters at the time of PAB due to variable volume status at the time of surgery. To improve the reproducibility of the surgical model system, a 20 ml/kg body weight fluid bolus was administered in the subsequent study between the surgical placement and tightening of the PAB.

UCB-Derived MNCs Promote a Dose-Dependent Increase of Proliferating Cardiomyocytes

Groups 2A, 2B, 2C. Fifteen animals receiving different UCB-MNCs doses [0.3 million cells/kg ($n = 5$), 1 million cells/kg ($n = 6$), and 3 million cells/kg ($n = 4$))] were sacrificed after 12 weeks of follow-up studies. Myocardial proliferation in the RV was studied in every group by immunohistochemistry staining for the proliferation markers Ki-67 and BrdU. Transplanted UCB-MNCs promoted a dose-dependent increase in proliferative activity in cardiomyocytes manifest as increased BrdU incorporation and increased Ki-67 positivity. Ki-67 expressing cells increased significantly from 2% $\pm$ 0.72% in the low-dose group (0.3 million cells/kg) to 4.1% $\pm$ 2.06% in the high-dose group (3 million cells/kg) (P-value <0.05, Fig. 4A–D). There were no statistical differences between the mid (1 million cells/kg) and high (3 million cells/kg) dose groups.

BrdU incorporation into proliferating cells was examined 24 h after injection. Eleven random photomicrographs were obtained from the histologic section of the RV-free wall taken from each animal and BrdU-positive cells were counted. The final count is the mean of the BrdU-positive cells per slide. As we saw with Ki-67 staining, BrdU nuclear staining significantly increased in a dose-dependent fashion, from 2.1 $\pm$ 0.53 cells/1.15 mm^2 in the 0.3 million cells/kg group versus 6.6 $\pm$ 2.92 cells/1.15 mm^2 in the 3 million cells/kg group (P-value $= 0.01$), and between the 0.3 million cells/kg group versus the 1 million cells/kg group (2.1 $\pm$ 0.53 cells/1.15 mm^2 vs 4.6 $\pm$ 2.24 cells/1.15 mm^2; P-value $= 0.04$). There were no statistical differences between the mid (1 million cells/kg) and high (3 million cells/kg) dose groups. The proliferating cells included cardiac and non-cardiac cells (Fig. 4E–H) (Fig S4).

Intramyocardial Delivery of UCB-MNCs Augment RV Remodeling Upon Chronic Pressure Overload

Groups 3A and 3B. The PAB surgery increased RV systolic pressure significantly from 70% to 90%. Two weeks post-banding, a mean Doppler gradient cutoff of 25 mm Hg across the PAB was used to screen for piglets with sufficient right ventricular dysfunction (Fig. 5B). During the 12-week follow-up after receiving the cell product at the highest dose (3 million cells/kg), the percentage increase in body weight was similar in the placebo and cell-treated groups (Fig. 5C). Animals grew from 6 to 7 kg initially to more than 40 kg by 12 weeks; the fixed band increased right ventricular pressure overload and produced a disease model sufficient to test the therapeutic potential of an autologous cell-based product. After 12 weeks of DMSO or UCB-MNCs injection, MRI was used to assess the structural and functional changes of the RV. There were no significant changes in RVEDV, RVESV, total pulmonary and systemic flow (QP, QS), effective ejection fraction (eEF), or cardiac output calculated by volumetric analysis and flow quantification between DMSO placebo and UCB-MNCs groups. The MRI scan parameters are listed in the supplementary section (Fig. S2). There was increased heart weight and RV wall thickness in UCB-MNCs treated animals at necropsy (Fig. 5D, E).

Myocardial Remodeling is Associated with Enhanced Cardiomyocyte Proliferation, Angiogenesis, and Regulation of Cardiac Specific Gene expression

Groups 3A and 3B. Immunohistochemistry staining showed a significant increase (~50%) in CD31+ expression in the RV after UCB-MNCs injection, compared with the placebo group (Fig. 6A–C).

To confirm that UCB-MNCs transplantation in the RV can increase cardiomyocyte proliferation compared to the placebo group, we analyzed Ki-67 reactive cells throughout the myocardium. These cells were confirmed to include cardiac myocytes by co-localization of Ki-67 with cardiac troponin (Fig. 6G–I). The significant increase in Ki-67 reactive cells in the RV myocardium was threefold higher than in the placebo group using automated software analysis (Fig. 6D–F). Of note, the LV was not affected by the RV injections, suggesting a localized effect of the intramyocardially transplanted product (data not shown). Furthermore, the UCB-MNCs injection to the RV of PAB animals resulted in a 13-fold up-regulation of the *WT1* gene. We also evaluated the gene expression levels of cardiogenic transcription factors including *Mef2c*, *NKX2.5*, and *GATA4*, and no statistically significant difference was observed. The gene expression analysis data are shown in the supplementary file (Fig. S3).

Discussion

Clinical management of severe CHD has undergone a persistent improvement over the past few decades, with more
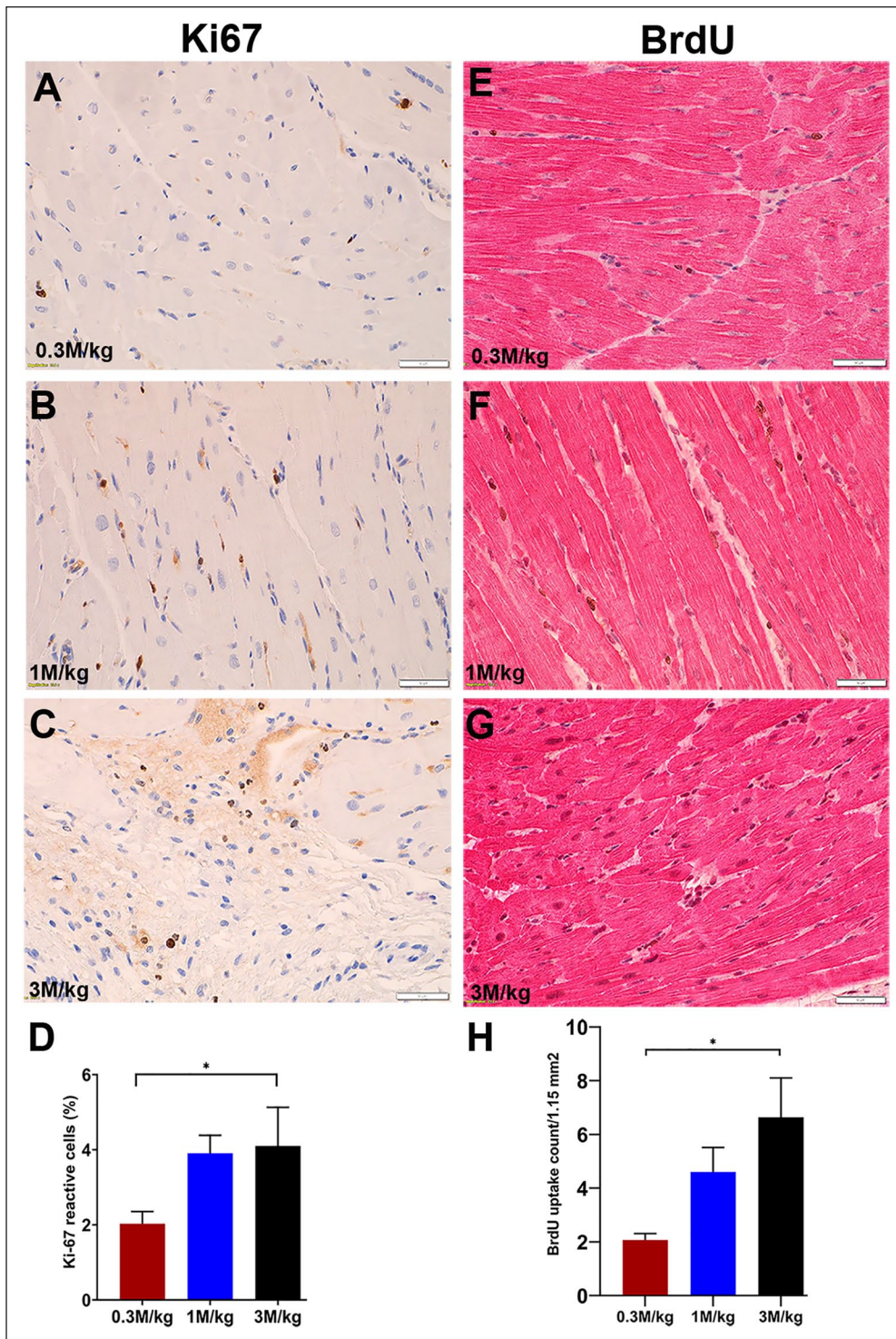
Figure 4. Autologous UCB-MNCs promote a dose-response activity of BrdU incorporation and the percentage of Ki-67 positive cells. (A–D) A dose-response increase of Ki-67 proliferation marker into myocardial cells. (E–G) Representative images and quantitative analysis of BrdU incorporated cells in the RV myocardium. At 12 weeks post cell transplantation with the highest dose (3 M/kg), the proliferation of the myocardial cells was significantly increased compared with the lowest dose (0.3 M/kg). (H) The BrdU incorporation into proliferating cells was well correlated with the Ki-67 proliferation index in a dose-dependent manner (*P value = 0.01). BrdU: bromodeoxyuridine; M/Kg: millions per kilogram; RV: right ventricle; UCB-MNCs: umbilical cord blood–derived mononuclear cells.
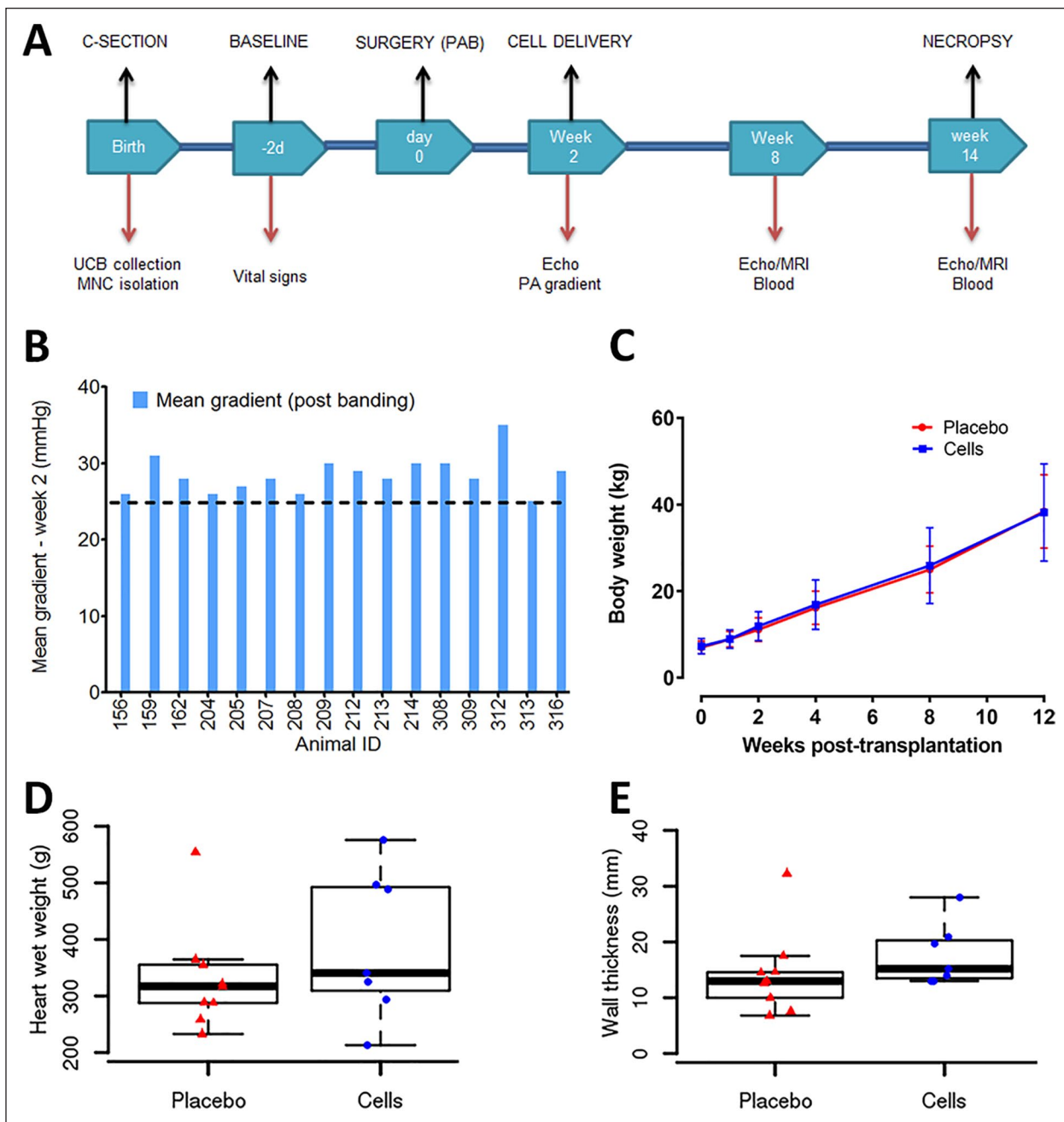
Figure 5. Double-blinded, randomized, placebo-controlled single high-dose UCB-MNCs efficacy study in chronic right ventricular pressure overload. (A) An overview of experimental design. (B) The mean gradient was monitored before banding. The pulmonary artery was constricted gradually and recorded the final RV pressure before closing the wound. Note one value was missing from animal 204. (C) Body weights were recorded at baseline, 2, 4, 6, 8, 10, and 12 weeks after cell delivery. No significant differences were seen between the two study groups. (D–E) Increased heart weight and wall thickness measured by Vernier calipers in UCB-MNCs treated animals at necropsy. C-section: cesarean section; DMSO: dimethyl sulfoxide; Echo: echocardiography; MNC: mononuclear cells; MRI: magnetic resonance imaging; PA: pulmonary artery; PAB: pulmonary artery banding; RV: right ventricle; UCB: umbilical cord blood.

adults now living with CHD than children as more individuals are surviving current surgical management[17]. The success is evident in single-ventricle palliation in hypoplastic left heart syndrome (HLHS)[4,18]. There are children and young adults that can thrive when the RV provides adequate cardiac output to meet their physiological demands. However, as cardiac demands increase with body growth and chronic pressure overload leads to maladaptive changes, heart failure
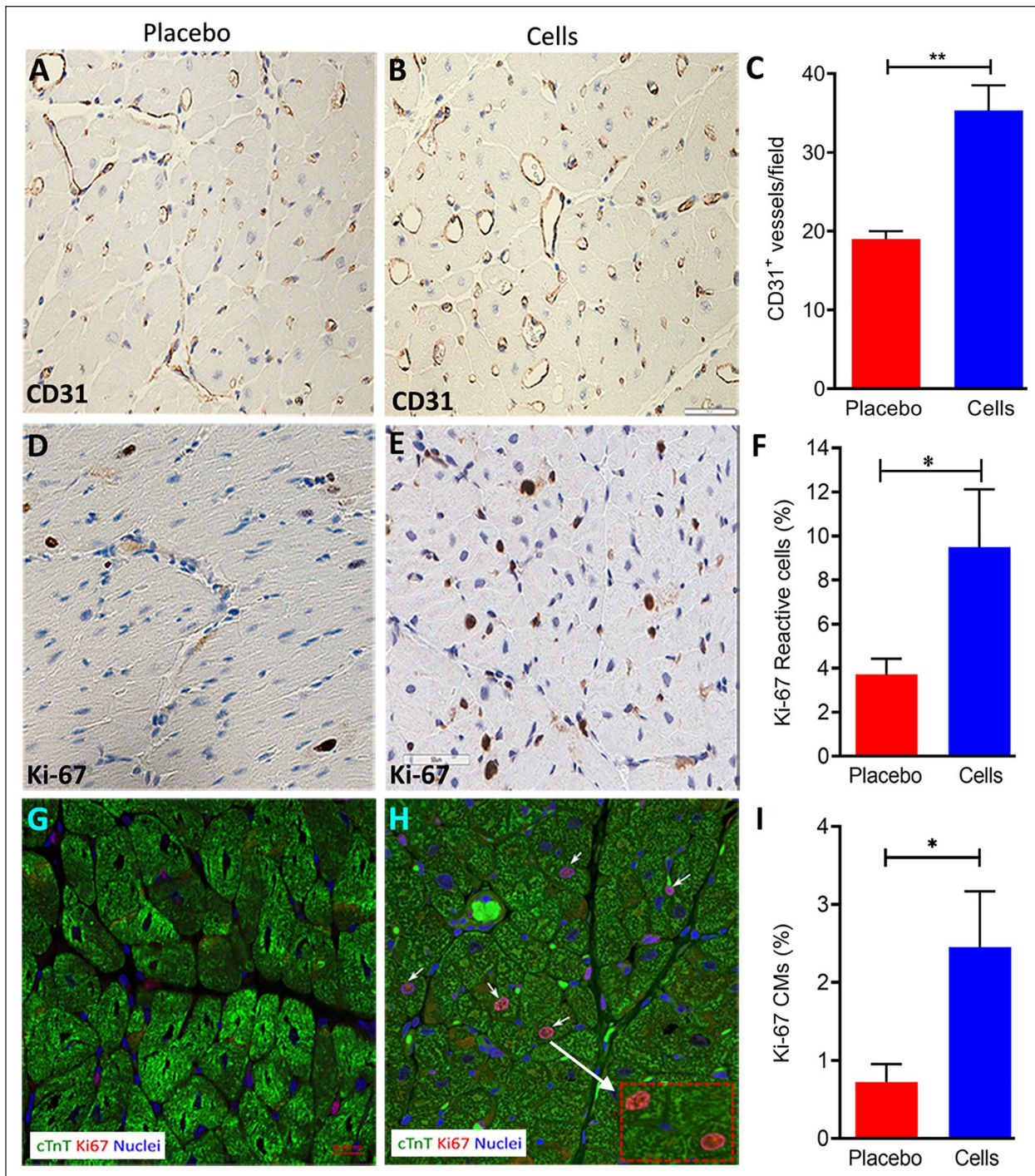
Figure 6. Proliferation and the angiogenic response of myocardium following intramyocardial delivery of a high dose of UCB-MNCs (3 million cells/kg). (A–C) Immunohistochemistry analysis for the angiogenesis marker CD31 was performed on paraffin-embedded cell-treated and PAB-only RV tissue. Vascularity in RV was assessed showing an increase in the number of CD31+ vessels after 12 weeks of cell delivery ($P = 0.01$ vs PAB, scale bars = 50 µM). (D–F) Immunohistochemistry images of Ki-67 staining in the free wall of RV from the placebo or UCB-cell group are illustrated. The percentage of Ki-67 reactive myocardial cells increased 2.5-fold in the UCB-MNCs group compared to the placebo group. (G–I) Representative photomicrographs showing immunofluorescence labeling of Ki-67 and cTnT in myocardial sections. The panel shows a significant increase of Ki-67 reactive cardiomyocytes in the myocardium (Ki-67+ cTnT+) in the UCB-MNCs group versus the placebo group (P value = 0.05). CMs: cardiomyocytes; cTnT: cardiac troponin T; MNC: mononuclear cells; PAB: pulmonary artery banding; RV: right ventricle; UCB: umbilical cord blood.

becomes a significant limitation for these individuals[19–22]. Therefore, sustaining cardiac performance and meeting the physiological demands of the entire cardiovascular system is of utmost importance to transform the clinical management of complex CHD[23]. Although there are multiple potential approaches to optimize outcomes for individual patients, preventing cardiac pump failure for Fontan patients could significantly affect long-term survival. Regenerative sciences have, in parallel, expanded our current understanding of how the myocardium develops, grows, and responds to lifelong stress. Today, there is a consensus that the myocardium undergoes self-renewal throughout its lifespan with the most dramatic growth potential in the neonatal and pediatric stages[24]. This is supported by a wide range of evidence in pre-clinical settings that indicate *de novo* myocardial growth originating from the innate cytokinesis of existing cardiomyocytes. Maximizing this natural process to augment cardiac function is an ongoing and active area of research that requires focused studies relating to pediatric stages of CHD[25]. A reproducible model system of juvenile right heart failure provides a pathway to evaluate therapeutic strategies aiming to recapitulate key features of the pediatric congenital heart.

PAB has been used in multiple studies to produce a failing RV in small and large animal models[26–30]. Herein, significant attention was applied to understanding the pathological response to PAB at juvenile developmental stages and establishing the most consistent model system to study pathological changes of the RV to allow effective randomization for therapeutic studies. The major lesson learned by the surgical team was the importance of avoiding atrial arrhythmias in the piglets by protecting the atria from unintentional stimulation. This proved to be potentially life-threatening given that anti-arrhythmic medications were deliberately withheld to maximize downstream sensitivities to safety concerns from experimental therapeutics. In addition, the standardization of the age of the piglets at surgery was potentially a critically important variable as pulmonary vascular resistance changes daily at this stage of development, yet this was not explicitly tested herein. Finally, fluid bolus was likely to be helpful to increase the reproducibility of the hemodynamic stress and the ability to tolerate a sufficiently tight band that would yield a reproducible pathological condition. Screening for a minimum PA gradient 2 weeks after surgery allowed for a better randomization process to avoid unaffected animals that would confound the study design of these relatively small cohort sizes. As the surgical team perfected the methodology and standardization of piglet care, it became expected that greater than 90% of the animals would survive the acute physiological demand and have a reproducible chronic RV pressure within the 12-week follow-up period. The piglet model is most useful in cardiovascular studies due to its similarity in cardiac anatomy and physiology to humans. Piglets start at a size nearly identical to the expected size of a human neonate with CHD and rapidly grow within 12 weeks to mimic almost a decade of human growth from a neonate to adolescent physiology. However, this fixed PAB model in rapidly growing animals can also cause erosions through the PA wall and create false lumens that bypass the band and dramatically change the hemodynamic stress, making it essential to eliminate these cases from the final analysis[31]. Thus, carefully controlled therapeutic studies require attention to the reproducibility of the model and validation of individual cases to avoid statistical outliers that can easily skew the analysis in small cohorts.

Cell-based therapies have been tested as a potential strategy to repair dysfunctional cardiac tissues in adults for the past decade, with mixed results in clinical trials[32–34]. One of the inherent limitations has been the lack of *de novo* cardiogenesis from the stem cell products and the limited ability of the host myocardium to be induced to undergo innate cardiogenesis from endogenous sources[24]. Although UCB is not thought to contribute to *de novo* cardiogenesis, the current understanding of cardiac biology predicts that paracrine-mediated induction of innate cardiogenesis could be more robust in pediatric settings than in elderly tissues[35]. However, cell-based therapies could also provoke unintended consequences given the risk of disrupting normal cardiac growth and differentiation. Therefore, the second part of this study aimed to establish the safety profile of a wide range of cell doses delivered into failing RV forced to compensate for physiological demands reminiscent of the single right ventricle in HLHS patients and to evaluate the effect of several concentrations of autologous UCB-derived cells on the proliferative activity of cardiomyocytes. This could be an ideal cohort for pediatric patients' cell-based therapeutic studies. Direct intramyocardial injection of cells into the RV was feasible in these banded subjects without evidence of structural, biochemical, or physiological adverse effects from any of the three doses used. The completion of clinical trials in humans is necessary to further assess the efficacy of autologous injection of UCB-MNCs to improve heart function in specific clinical conditions.

The myocardium has the ability to grow in the pediatric and adolescent stages of mammalian development but gives way to a hypertrophic response later in life. BrdU was administered intravenously in all animals after 12 weeks post-cell injection to label and track proliferating myocardial cells. Subsequently, all animals from every cell dose group were sacrificed 24 h after BrdU injection. Incorporation of BrdU in cardiac and non-cardiac cells in RV was most extensive in the group of animals that received 3×10^6 TNC/kg compared to the group that received 10 times less concentration of autologous umbilical cord blood cells. Identical results were observed when the Ki-67 proliferation marker was assessed in the same subset of RV samples. This shows a reproducible dose-dependent response in myocardial proliferation, which we hypothesize is most likely from the paracrine effect induced by UCB-MNCs. Therefore, the third study presented herein was designed to examine the impact of cell-based delivery using 3×10^6 TNC/kg versus

placebo into the myocardium of piglets to confirm if innate cardiac regenerative mechanisms are augmented within a time range similar to the period when CHD patients would typically undergo a bidirectional cavopulmonary shunt for single-ventricle palliation. Although the post-therapeutic hemodynamics were not significantly changed given this surgical model system, we examined the molecular and histological evidence of cardiac regeneration following UCB-MNCs delivery according to established approaches now applied to the piglet model system herein[25]. As we observed in the second part of the study using Ki-67 immunohistochemistry, proliferative activity in cardiomyocytes of the RV was increased in a statistically significant fashion in the cell-treated group, confirming that proliferation of cardiomyocytes is augmented when UCB-MNCs were injected at 3×10^6 TNCs/kg. This would explain the increased heart weight and wall thickness observed in the animals 12 weeks after receiving UCB-MNCs. Sano et al. showed an increased ventricular mass index (ventricular mass/body surface area) in the LV type (139 ± 42 g/m²) versus the RV type (99 ± 36 g/m²), which explained the better LV type of univentricular heart adaptation, as a higher EF[5]. An inadequate compensatory ventricular hypertrophy could result in abnormal function and contractility. The RVs had a decreased mean EF after bidirectional cavopulmonary connection (BDCPC) compared with single morphologic LVs, which remained stable[5,6,36]. Moreover, Vincenti et al. recently published similar results, especially in the HLHS population subset[37].

The gene expression profile demonstrated the induction of pro-regenerative genes such as *WT1*, which is known to be expressed in epicardial cells that function as progenitors for both coronary artery development and *de novo* myocardial cells with predominance in the left ventricle[38–41]. Furthermore, *WT1*-reactive cells have been directly linked to *de novo* cardiogenesis and *in vivo* production of functional cardiomyocytes[42,43]. They are consistent with the emerging paradigm of the importance of the epicardium in cardiac growth[44–46]. However, the cardiac expression of Wt1 does not belong exclusively to the cells from the epicardium. Some studies illustrate during heart development and after acute myocardial ischemia a characteristic Wt1 expression in endothelial cells, being its expression higher in those endothelial cells that are actively proliferating, and can augment the vascular endothelial growth factor (VEGF) expression, an angiogenic factor involved in regenerative processes[45,47–49]. Bauer et al. describe that immediate early gene expression and pro-angiogenic gene expression are induced by PAB alone[50]. Yet, using PAB as the blinded randomized control, we now recognize the additional impact of UCB-MNCs on this underlying profile and the specific induction of *WT1*-associated processes. Validating this proliferative impact of UCB-MNC injections, histological analysis using standardized techniques within clinical pathology workflows demonstrated increased Ki-67 expression specifically in the host tissues that received the UCB-MNCs. Furthermore, our study showed an increase in the number of CD31+ vessels after 12 weeks of UCB-MNCs delivery. The data show that the increased vasculature may play a crucial role in maintaining heart function by promoting angiogenesis. It is known that the expression of PECAM-1 (CD31) and c-kit are transcriptionally controlled by the upregulated *Wt1* gene[51]. Altogether, these data indicate that the known ability of resident cardiac cells to proliferate within pediatric hearts can be augmented in response to the intramyocardial delivery of UCB-MNCs threefold over sham controls. Furthermore, several pre-clinical animal and clinical studies have shown that age could interfere with the functions and potency of progenitor cells[52,53]. Stem cells from younger individuals have been shown to be more naive and plastic than stem cells from adults[35,54] and thus could explain the induction of a measurable pro-regenerative response in this juvenile model system.

Altogether, this work demonstrates that UCB-derived cells could enhance myocardial proliferation and initiate myocardial angiogenesis, both necessary for an adaptive regenerative response. Moreover, the cell concentration of at least 1×10^6 UCB cells/kg delivered into the RV showed a significant myocardial proliferation augmentation compared with the lowest dose (0.3×10^6 UCB cells/kg) or placebo with no safety issues. Therefore, this suggests that a higher TNC dose may be used in clinical trials to achieve the most potent effects in pediatric patients with CHD, though this will need to be confirmed with appropriate clinical safety studies. Ultimately, it is hoped that this intervention may promote myocardial proliferation in humans with CHD as well, leading to a better ventricular adaptation due to an adequate ratio of ventricular mass to end-diastolic volume.

Limitations

Standardization of a complex surgical disease model is difficult as individuals may respond to the same stimulus in different ways complicating the assessment of the efficacy of UCB-MNCs. The permanent PAB poses a fixed obstruction and increased right ventricular afterload which is supra-systemic in nature. Without directly modifying the pressure gradient, this model is unlikely to detect modulation of cardiac performance, and thus this surgical model system is not ideal to quantify increased contractility of the myocardium with experimental therapies alone. Small numbers or dropouts related to the early death of animals in certain groups and the presence of outliers in some groups substantially limit the processes of estimating statistical significance. Limitations were the small sample size for the measurement of echocardiography and MRI. The echocardiography and MRI of the RV is challenging; in contrast to LV, the echocardiography data of RV size and function may not always be feasible or reproduce the data.

Conclusion

Collectively, these studies establish a reproducible surgical model system to recapitulate RV features of a single-ventricle cardiovascular system in a juvenile setting. The safety and feasibility of intramyocardial delivery of an autologous MNCs product in RV was validated in this pressure overload model system. Finally, the efficacy of UCB-MNCs delivery within a chronic pressure overloaded RV indicates the ability of an autologous cell-based product to augment cellular proliferation and adaptation of the stressed myocardium. These studies highlight the importance of ongoing pre-clinical studies to focus on molecular markers of cardiac regeneration beyond the short-term structural performance of the myocardium alone. Furthermore, these studies highlight the need to define the regenerative response of the pediatric myocardium to understand the full potential of this paracrine-mediated effect and optimize the frequency and timing of cell-based therapeutic strategies.

Author Contributions

SO, SCP, and MYQ contributed equally to this manuscript in study design, manuscript writing, data analysis, and data interpretation. MYQ performed MRI, analysis, and data interpretation. KAH, BSE, and EBB made contributions to data acquisition and analysis. HMB and JAD executed surgical procedures. MAH and WKK performed the statistical analysis. BTL and JJM performed the histological examination, analysis, and interpretation. TJN made financial support, cell transplantation, and final approval of the manuscript. Wanek Program Pre-Clinical Pipeline: data collection and technical assistance.

Ethical Approval

Ethical approval to conduct this study was obtained from the Institutional Animal Care and Use Committee (IACUC) of Mayo Clinic, Rochester, MN, protocols (A18313-13; 00001782-16 and A00004884-19).

Statement of Human and Animal Rights

All animal study protocols and SOPs were conducted under the regulations and guidelines of IACUC, Mayo Clinic, Rochester, MN.

Statement of Informed Consent

The research data did not constitute any human subjects and informed consent is not applicable.

Declaration of Conflicting Interests

The author(s) declared no potential conflicts of interest with respect to the research, authorship, and/or publication of this article.

ORCID iDs

Saji Oommen (iD) https://orcid.org/0000-0001-6824-4894

Muhammad Y. Qureshi (iD) https://orcid.org/0000-0002-9898-2318

Emma B. Brandt (iD) https://orcid.org/0000-0003-3135-4314

Supplemental Material

Supplemental material for this article is available online.

References

1. van der Linde D, Konings EE, Slager MA, Witsenburg M, Helbing WA, Takkenberg JJ, Roos-Hesselink JW. Birth prevalence of congenital heart disease worldwide: a systematic review and meta-analysis. J Am Coll Cardiol. 2011;58(21):2241–47.

2. Bouma BJ, Mulder BJM. Changing landscape of congenital heart disease. Circ Res. 2017;120(6):908–22.

3. Ohye RG, Ludomirsky A, Devaney EJ, Bove EL. Comparison of right ventricle to pulmonary artery conduit and modified Blalock-Taussig shunt hemodynamics after the Norwood operation. Ann Thorac Surg. 2003;78(3):1090–93.

4. Pizarro C, Mroczek T, Malec E, Norwood WI. Right ventricle to pulmonary artery conduit reduces interim mortality after stage 1 Norwood for hypoplastic left heart syndrome. Ann Thorac Surg. 2004;78(6):1959–63; discussion 63–4.

5. Sano T, Ogawa M, Taniguchi K, Matsuda H, Nakajima T, Arisawa J, Shimazaki Y, Nakano S, Kawashima Y. Assessment of ventricular contractile state and function in patients with univentricular heart. Circulation. 1989;79(6):1247–56.

6. Kaneko S, Khoo NS, Smallhorn JF, Tham EB. Single right ventricles have impaired systolic and diastolic function compared to those of left ventricular morphology. J Am Soc Echocardiogr. 2012;25(11):1222–30.

7. Tabarsi N, Guan M, Simmonds J, Toma M, Kiess M, Tsang V, Ruygrok P, Konstantinov I, Shi W, Grewal J. Meta-analysis of the effectiveness of heart transplantation in patients with a failing Fontan. Am J Cardiol. 2017;119(8):1269–74.

8. Burkhart HM, Qureshi MY, Rossano JW, Cantero Peral S, O'Leary PW, Hathcock M, Kremers W, Nelson TJ. Autologous stem cell therapy for hypoplastic left heart syndrome: safety and feasibility of intraoperative intramyocardial injections. J Thorac Cardiovasc Surg. 2019;158(6):1614–23.

9. Cantero Peral S, Burkhart HM, Oommen S, Yamada S, Nyberg SL, Li X, O'Leary PW, Terzic A, Cannon BC, Nelson TJ. Safety and feasibility for pediatric cardiac regeneration using epicardial delivery of autologous umbilical cord blood-derived mononuclear cells established in a porcine model system. Stem Cells Transl Med. 2015;4(2):195–206.

10. Harris DT, Rogers I. Umbilical cord blood: a unique source of pluripotent stem cells for regenerative medicine. Curr Stem Cell Res Ther. 2007;2(4):301–309.

11. Wairiuko GM, Crisostomo PR, Wang M, Morrell ED, Meldrum KK, Lillemoe KD, Meldrum DR. Stem cells improve right ventricular functional recovery after acute pressure overload and ischemia reperfusion injury. J Surg Res. 2007;141(2):241–46.

12. Yerebakan C, Sandica E, Prietz S, Klopsch C, Ugurlucan M, Kaminski A, Abdija S, Lorenzen B, Boltze J, Nitzsche B, Egger D, et al. Autologous umbilical cord blood mononuclear cell transplantation preserves right ventricular function in a novel model of chronic right ventricular volume overload. Cell Transplant. 2009;18(8):855–68.

13. Achyut BR, Varma NR, Arbab AS. Application of umbilical cord blood derived stem cells in diseases of the nervous system. J Stem Cell Res Ther. 2014;4:1000202.

14. Markov V, Kusumi K, Tadesse MG, William DA, Hall DM, Lounev V, Carlton A, Leonard J, Cohen RI, Rappaport EF, Saitta B. Identification of cord blood-derived mesenchymal stem/stromal cell populations with distinct growth kinetics, differentiation potentials, and gene expression profiles. Stem Cells Dev. 2007;16(1):53–73.

15. Peters EB, Liu B, Christoforou N, West JL, Truskey GA. Umbilical cord blood-derived mononuclear cells exhibit pericyte-like phenotype and support network formation of endothelial progenitor cells in vitro. Ann Biomed Eng. 2015; 43(10):2552–68.

16. Wyrsch A, dalle Carbonare V, Jansen W, Chklovskaia E, Nissen C, Surbek D, Holzgreve W, Tichelli A, Wodnar-Filipowicz A. Umbilical cord blood from preterm human fetuses is rich in committed and primitive hematopoietic progenitors with high proliferative and self-renewal capacity. Exp Hematol. 1999;27(8):1338–45.

17. Gilboa SM, Devine OJ, Kucik JE, Oster ME, Riehle-Colarusso T, Nembhard WN, Xu P, Correa A, Jenkins K, Marelli AJ. Congenital heart defects in the United States: estimating the magnitude of the affected population in 2010. Circulation. 2016;134(2):101–109.

18. Ohye RG, Schranz D, D'Udekem Y. Current therapy for hypoplastic left heart syndrome and related single ventricle lesions. Circulation. 2016;134(17):1265–79.

19. Downing TE, Allen KY, Glatz AC, Rogers LS, Ravishankar C, Rychik J, Faerber JA, Fuller S, Montenegro LM, Steven JM, Spray TL, et al. Long-term survival after the Fontan operation: twenty years of experience at a single center. J Thorac Cardiovasc Surg. 2017;154(1):243–53.

20. Pundi KN, Johnson JN, Dearani JA, Pundi KN, Li Z, Hinck CA, Dahl SH, Cannon BC, O'Leary PW, Driscoll DJ, et al. 40-Year follow-up after the Fontan operation. J Am Coll Cardiol. 2015;66(15):1700–10.

21. Carins TA, Shi WY, Iyengar AJ, Nisbet A, Forsdick V, Zannino D, Gentles T, Radford DJ, Justo R, Celermajer DS, Bullock A, et al. Long-term outcomes after first-onset arrhythmia in Fontan physiology. J Thorac Cardiovasc Surg. 2016;152(5):1355–63.

22. Pundi KN, Pundi KN, Johnson JN, Dearani JA, Li Z, Driscoll DJ, Wackel PL, McLeod CJ, Cetta F, Cannon BC. Sudden cardiac death and late arrhythmias after the Fontan operation. Congenit Heart Dis. 2017;12(1):17–23.

23. Rychik J. The relentless effects of the Fontan paradox. Semin Thorac Cardiovasc Surg Pediatr Card Surg Annu. 2016;19(1): 37–43.

24. Eschenhagen T, Bolli R, Braun T, Field LJ, Fleischmann BK, Frisén J, Giacca M, Hare JM, Houser SR, Lee RT, et al. Cardiomyocyte regeneration: a consensus statement. Circulation. 2017;136:680–86.

25. Galdos FX, Guo Y, Paige SL, VanDusen NJ, Wu SM, Pu WT. Cardiac regeneration. *lessons from Development*. Circ Res. 2017;120(6):941–59.

26. Hyldebrandt JA, Sivén E, Agger P, Frederiksen CA, Heiberg J, Wemmelund KB, Ravn HB. Effects of milrinone and epinephrine or dopamine on biventricular function and hemodynamics in an animal model with right ventricular failure after pulmonary artery banding. Am J Physiol Heart Circ Physiol. 2015;309(1): H206–12.

27. Wehman B, Sharma S, Pietris N, Mishra R, Siddiqui OT, Bigham G, Li T, Aiello E, Murthi S, Pittenger M, et al. Mesenchymal stem cells preserve neonatal right ventricular function in a porcine model of pressure overload. Am J Physiol Heart Circ Physiol. 2016;310(11): H1816–26.

28. Vikholm P, Schiller P, Hellgren L. A modified Glenn shunt reduces venous congestion during acute right ventricular failure due to pulmonary banding: a randomized experimental study. Interact Cardiovasc Thorac Surg. 2014;18(4):418–25.

29. Lambert V, Capderou A, Le Bret E, Rücker-Martin C, Deroubaix E, Gouadon E, Raymond N, Stos B, Serraf A, Renaud JF. Right ventricular failure secondary to chronic overload in congenital heart disease: an experimental model for therapeutic innovation. J Thorac Cardiovasc Surg. 2010;139(5):1197–1204; 1204.e1.

30. Oommen S, Yamada S, Cantero Peral S, Campbell KA, Bruinsma ES, Terzic A, Nelson TJ. Human umbilical cord blood-derived mononuclear cells improve murine ventricular function upon intramyocardial delivery in right ventricular chronic pressure overload. Stem Cell Res Ther. 2015;6(1):50.

31. Jalal Z, Roubertie F, Fournier E, Dubes V, Benoist D, Naulin J, Delmond S, Durand M, Haissaguerre M, Bernus O, Thambo JB. Unexpected internalization of a pulmonary artery band in a porcine model of Tetralogy of Fallot. World J Pediatr Congenit Heart Surg. 2017;8(1):48–54.

32. Assmus B, Honold J, Schächinger V, Britten MB, Fischer-Rasokat U, Lehmann R, Teupe C, Pistorius K, Martin H, Abolmaali ND, et al. Transcoronary transplantation of progenitor cells after myocardial infarction. N Engl J Med. 2006; 355(12):1222–32.

33. Bartunek J, Vanderheyden M, Vandekerckhove B, Mansour S, De Bruyne B, De Bondt P, Van Haute I, Lootens N, Heyndrickx G, Wijns W. Intracoronary injection of CD133-positive enriched bone marrow progenitor cells promotes cardiac recovery after recent myocardial infarction: feasibility and safety. Circulation. 2005;112(9 Suppl): I178–83.

34. Losordo DW, Henry TD, Davidson C, Sup Lee J, Costa MA, Bass T, Mendelsohn F, Fortuin FD, Pepine CJ, Traverse JH, et al. Intramyocardial, autologous CD34+ cell therapy for

refractory angina/novelty and significance. Circ Res. 2011;109(4):428–36.

35. Traister A, Patel R, Huang A, Patel S, Plakhotnik J, Lee JE, Medina MG, Welsh C, Ruparel P, Zhang L, et al. Cardiac regenerative capacity is age- and disease-dependent in childhood heart disease. PLOS ONE. 2018;13(7):e0200342.

36. Suntratonpipat S, Khoo NS, Colen T, Alhabdan M, Troung D, Zahari N, Kutty S, Smallhorn JF, Tham EB. Impaired single right ventricular function compared to single left ventricles during the early stages of palliation: a longitudinal study. J Am Soc Echocardiogr. 2017;30(5):468–77.

37. Vincenti M, Qureshi MY, Niaz T, Seisler DK, Nelson TJ, Cetta F. Loss of ventricular function after bidirectional cavopulmonary connection: who is at risk? Pediatr Cardiol. 2020;41:1714–24.

38. Wagner N, Wagner K-D, Theres H, Englert C, Schedl A, Scholz H. Coronary vessel development requires activation of the TrkB neurotrophin receptor by the Wilms' tumor transcription factor Wt1. Genes Dev. 2005;19(21):2631–42.

39. von Gise A, Zhou B, Honor LB, Ma Q, Petryk A, Pu WT. WT1 regulates epicardial epithelial to mesenchymal transition through β-catenin and retinoic acid signaling pathways. Dev Biol. 2011;356(2):421–31.

40. Bock-Marquette I, Shrivastava S, Teg Pipes GC, Thatcher JE, Blystone A, Shelton JM, Galindo CL, Melegh B, Srivastava D, Olson EN, et al. Thymosin β4 mediated PKC activation is essential to initiate the embryonic coronary developmental program and Epicardial progenitor cell activation in adult mice in vivo. J Mol Cell Cardiol. 2009;46(5):728–38.

41. Vicente-Steijn R, Scherptong RW, Kruithof BP, Duim SN, Goumans MJ, Wisse LJ, Zhou B, Pu WT, Poelmann RE, Schalij MJ, Tallquist MD, et al. Regional differences in WT-1 and Tcf21 expression during ventricular development: implications for myocardial compaction. PLOS ONE. 2015;10(9):e0136025.

42. Zhou B, Ma Q, Rajagopal S, Wu SM, Domian I, Rivera-Feliciano J, Jiang D, von Gise A, Ikeda S, Chien KR, et al. Epicardial progenitors contribute to the cardiomyocyte lineage in the developing heart. Nature. 2008;454(7200):109–13.

43. Smart N, Bollini S, Dubé KN, Vieira JM, Zhou B, Davidson S, Yellon D, Riegler J, Price AN, Lythgoe MF, et al. De novo cardiomyocytes from within the activated adult heart after injury. Nature. 2011;474(7353):640–44.

44. Smits AM, Riley PR. Epicardium-derived heart repair. J Dev Biol. 2014;2(2):84–100.

45. Duim SN, Kurakula K, Goumans MJ, Kruithof BP. Cardiac endothelial cells express Wilms' tumor-1. J Mol Cell Cardiol. 2015;81:127–35.

46. Martinez-Estrada OM, Lettice LA, Essafi A, Guadix JA, Slight J, Velecela V, Hall E, Reichmann J, Devenney PS, Hohenstein P, Hosen N, et al. Wt1 is required for cardiovascular progenitor cell formation through transcriptional control of Snail and E-cadherin. Nat Genet. 2010;42(1):89–93.

47. Aguiar C, Brunt KR. Wilms' tumor 1 (re)activation in evidence for both epicardial progenitor and endothelial cells for cardiovascular regeneration. J Mol Cell Cardiol. 2015;84:112–15.

48. McCarty G, Awad O, Loeb DM. WT1 protein directly regulates expression of vascular endothelial growth factor and is a mediator of tumor response to hypoxia. J Biol Chem. 2011;286(51):43634–43.

49. Xiang FL, Liu Y, Lu X, Jones DL, Feng Q. Cardiac-specific overexpression of human stem cell factor promotes epicardial activation and arteriogenesis after myocardial infarction. Circ Heart Fail. 2014;7(5):831–42.

50. Bauer EP, Kuki S, Arras M, Zimmerman R, Schaper W. Increased growth factor transcription after pulmonary artery banding. Eur J Cardiothorac Surg. 1997;11(5):818–23.

51. Wagner KD, Cherfils-Vicini J, Hosen N, Hohenstein P, Gilson E, Hastie ND, Michiels JF, Wagner N. The Wilms' tumour suppressor Wt1 is a major regulator of tumour angiogenesis and progression. Nat Commun. 2014;5:5852.

52. Dimmeler S, Leri A. Aging and disease as modifiers of efficacy of cell therapy. Circ Res. 2008;102(11):1319–30.

53. Flores I, Blasco MA. The role of telomeres and telomerase in stem cell aging. FEBS Lett. 2010;584(17):3826–30.

54. Agarwal U, Smith AW, French KM, Boopathy AV, George A, Trac D, Brown ME, Shen M, Jiang R, Fernandez JD, Kogon BE, et al. Age-dependent effect of pediatric cardiac progenitor cells after juvenile heart failure. Stem Cells Transl Med. 2016;5(7):883–92.